We are IntechOpen, the world's leading publisher of Open Access books
Built by scientists, for scientists

4,800
Open access books available

122,000
International authors and editors

135M
Downloads

Our authors are among the

154
Countries delivered to

TOP 1%
most cited scientists

12.2%
Contributors from top 500 universities

CLARIVATE ANALYTICS
BOOK CITATION INDEX
INDEXED

WEB OF SCIENCE™

Selection of our books indexed in the Book Citation Index in Web of Science™ Core Collection (BKCI)

Interested in publishing with us?
Contact book.department@intechopen.com

Numbers displayed above are based on latest data collected.
For more information visit www.intechopen.com

Chapter 7

Electric Field of a Medium Voltage Indoor Post Insulator

Mirza Sarajlić, Jože Pihler, Nermin Sarajlić and Peter Kitak

Additional information is available at the end of the chapter

http://dx.doi.org/10.5772/intechopen.71871

Abstract

This chapter deals with the influence of the electric field on a Medium Voltage Indoor Post Insulator (MVIPI) with standard and modified external shapes. The goal of this chapter is to show the electric field behavior of the MVIPI with different external shapes and to introduce a numerical model with a favorable distribution of the electric field that relieves the dielectric from stress. The chapter describes an MVIPI with nominal voltage 20 kV AC and shows an existing MVIPI, an MVIPI with a different number of ribs, and an MVIPI with exceptional external shape. The MVIPI's new external shape does not have the typical shape of the ribs, but a new outline, using the Lagrange polynomial, that will acquire its optimal form through the optimization process. A Differential Evolution optimization algorithm is used for the optimal design of the insulator's external shape. The value of the Electric Field Strength (EFS) will be minimized within the permissible bounds during the optimization process. The important parameters during the minimization of the objective function are the value of the EFS in the interior and exterior of the insulator. EFS values are shown for every MVIPI example and are compared with the existing MVIPI. The obtained results are analyzed and discussed.

Keywords: electric field, medium voltage, indoor post insulator, shape, optimization

1. Introduction

Medium voltage indoor post insulators (MVIPIs) are the most common elements used in switchgear [1]. They are the significant components of electric power devices [2]. Electric insulation of conductive parts from the grounded parts is the primary task of the insulator [3].

IntechOpen

© 2018 The Author(s). Licensee IntechOpen. This chapter is distributed under the terms of the Creative Commons Attribution License (http://creativecommons.org/licenses/by/3.0), which permits unrestricted use, distribution, and reproduction in any medium, provided the original work is properly cited. CC BY

Porcelain was used firstly as an insulator's material. Various epoxy resins appeared in the mid-60s, combined with various binders, glues, and fillers. Composite insulators are being produced increasingly recently for indoor and outdoor mounting. Araldite MVIPI (**Figure 1a**) is most used for internal mounting and has great insulation, mechanical, and thermic properties. With small dimensions, the MVIPI has a compound form and long lifespan [4].

The insulator model was built in MATLAB software, which has a dual task. Firstly, MATLAB does the task of a preprocessor, which is described in Section 2. MATLAB's second task is application of the optimization process. The selected optimization algorithm Differential Evolution (DE) [5, 6] is written and executed in MATLAB, which is described in Section 5, where the minimization of the objective function has been implemented. The essential parameter of the objective function is the value of EFS in the interior and exterior of the insulator. During the optimization process, the value of the EFS will be reduced within the admissible bounds and will be calculated using EleFAnT software [7].

The chapter is organized as follows. An existing MVIPI model is described in Section 2. Section 3 describes the MVIPI with a different number of ribs. Section 4 describes the novel-designed MVIPI using the Lagrange polynomial. The optimization calculation of the MVIPI's external shape and the best position of internal insulator components using DE algorithm is described in Section 5, with the Conclusion given in Section 6.

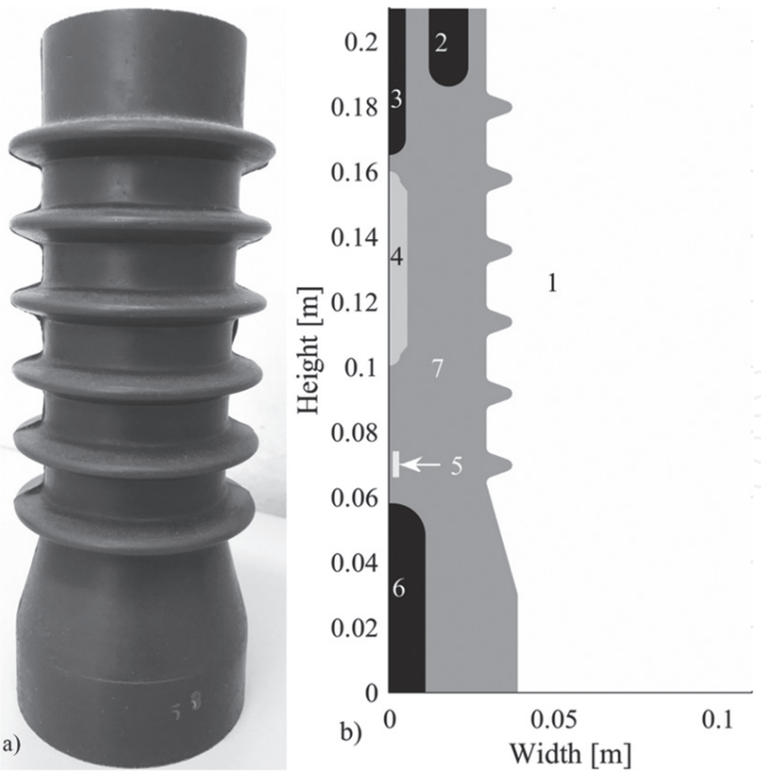

Figure 1. (a) Existing MVIPI and (b) MVIPI model in program tool MATLAB.

2. MVIPI model

The existing MVIPI has six ribs (**Figure 1**). The MVIPI's parts are labeled with the numbers stated in **Table 1**, which also shows the materials and the potentials of each component required for the calculation of the electric field.

The complete MVIPI model geometry is generated using a mesh generator, which is part of the preprocessor. The mesh generator distributes the whole problem area into finite elements [8–10], which are isoparametric quadrangular elements in the case of axisymmetric model. The problem is separated into single geometric shapes that belong to respective types of material. There are seven geometric shapes: surrounding area (1), upper right connector (2), upper indicator electrode (3), capacitor (4), resistor (5), bottom electrode (6), and insulation material (7).

The upper right connector and upper indicator electrode are connected to high voltage. Their function is to connect the conductor (i.e., contact, busbar) on the insulator. The bottom electrode is grounded and functions to attach the insulator on grounded infrastructure (i.e., cells' housing).

The ceramic capacitor helps in achieving appropriate capacitance, defined by Standards IEC 61958 [11] and IEC 61243–5 [12]. The capacitance must be between 74 and 88 pF, according to [11, 12]. The electric field in the air and the outside surface of the MVIPI has to be less than 3 MV/m and inside the insulator less than 30 MV/m.

The MVIPI's designing requires input data, such as insulator geometry, materials, and boundary conditions. Potential's value passes from the source potential (upper indicator electrode) to the grounded part (bottom electrode). The Dirichlet boundary condition 0 V is on the right edge of the MVIPI's model. The material is described by means of the dielectric permittivity, which, for araldite, is $\varepsilon_{r,araldite} = 4.3$ and, for the air, $\varepsilon_{r,air} = 1$. The MVIPI model is written parametrically, which enables the rapid adjustment of geometry and full control of materials, potential, and boundary conditions. Finding the best parameters is executed with an iterative process of updating the MVIPI model with new input parameters.

Number	Geometric shape	Material	Potential
1	Surrounding area	Air	Floating potential
2	Upper right connector	Metal	125 kV DC[1]
3	Upper indicator electrode	Metal	125 kV DC[1]
4	Capacitor	Ceramics	Floating potential
5	Resistor	Metal	Floating potential
6	Bottom electrode	Metal	0 V
7	Insulation material	Araldite	Floating potential

[1]20 kV MVIPI must endure 125 kV DC as the maximum test voltage (lightning impulse voltage).

Table 1. Explanation of geometric shapes from **Figure 1**.

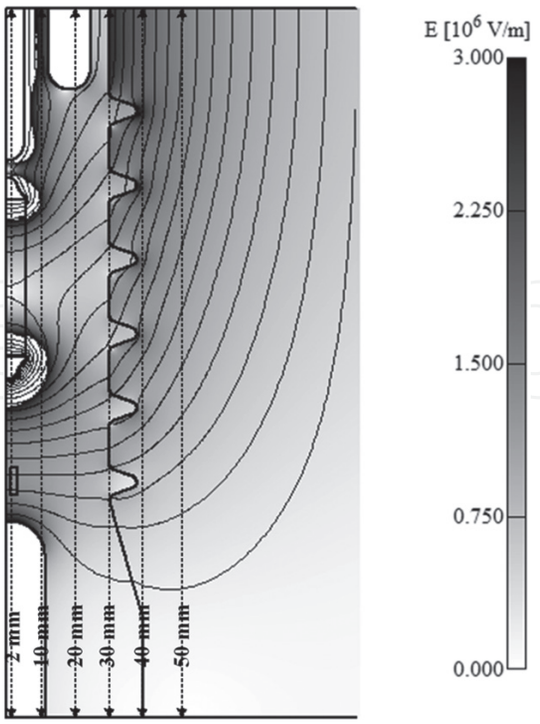

Figure 2. EFS of the existing MVIPI.

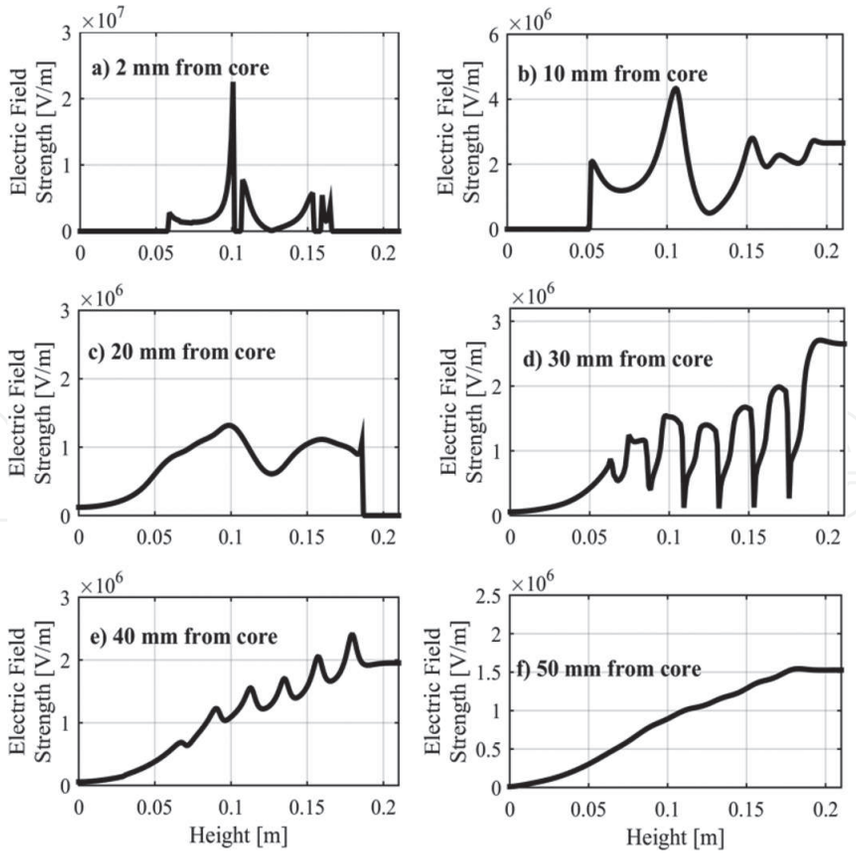

Figure 3. EFS of the existing MVIPI at different distances from the core of the MVIPI: (a) 2 mm for core, (b) 10 mm from core, (c) 20 mm from core, (d) 30 mm from core, (e) 40 mm from core and (f) 50 mm from core.

Figure 2 shows a plot of the existing MVIPI's EFSs. **Figure 3** shows EFSs at different distances from the core of the MVIPI. As is apparent in **Figure 3**, the values of EFS are within the defined bounds (at 2, 10, and 20 mm), the dielectric strength is not exceeded (30 MV/m). Also, there was no excess of the EFS (3 MV/m) in the air (at 30, 40, and 50 mm).

3. MVIPI with a lower and higher number of ribs

Modeling of the MVIPI's exterior is presented in the following. Examples of an MVIPI with lower and higher number of ribs are shown and compared with the existing MVIPI. **Figure 4a** shows the EFS of the MVIPI with five ribs. **Figure 4b** shows the EFS of the MVIPI with nine ribs. **Figure 5** shows the comparison of the EFS between the existing MVIPI and MVIPIS with five and nine ribs at different distances from the core of the MVIPI.

The EFS of the MVIPI with five ribs is marked with a dotted line (**Figure 5**); a solid line marks the EFS with nine ribs, and a dashed line represents the EFS of the existing MVIPI. There is no significant change in the electric field in the interior of the insulator (**Figure 5a–5c**). The EFS values in **Figure 5d** and **5e** are approximately equal; the electric field is distributed better at the insulator with nine ribs. The differences between EFS values are negligibly small in **Figure 5f**.

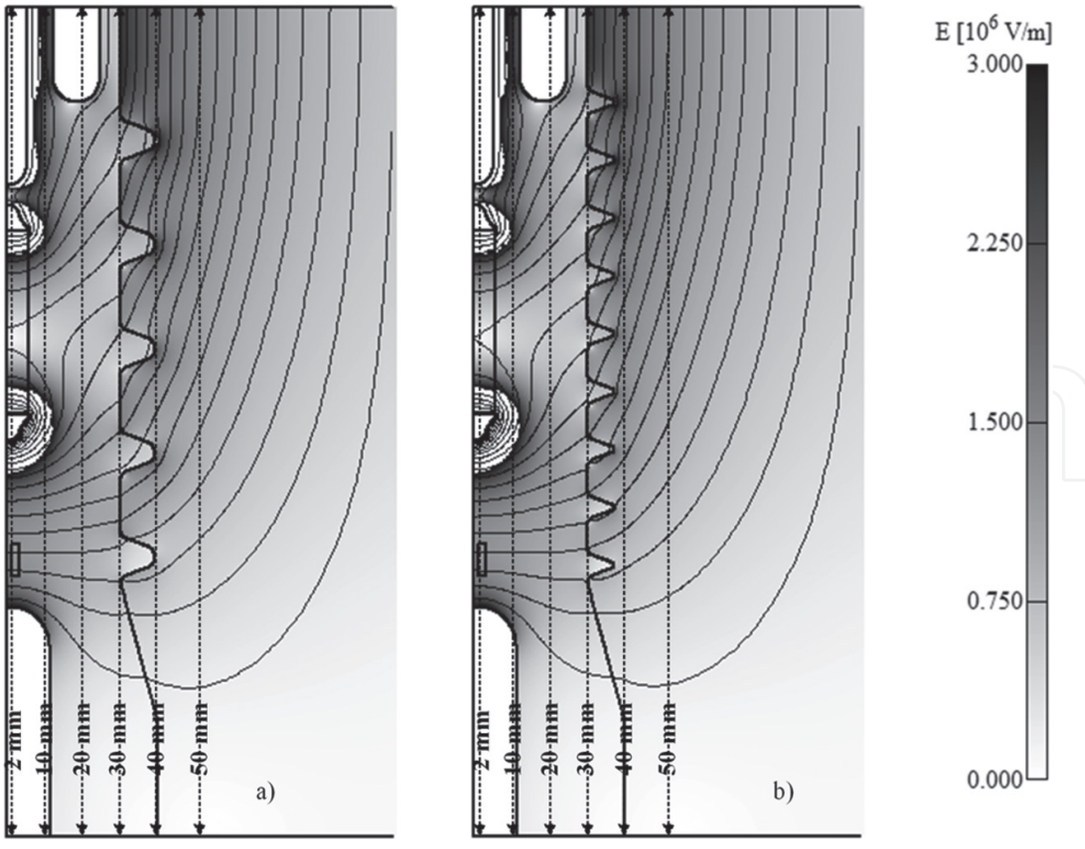

Figure 4. EFS of the MVIPI with: (a) five ribs and (b) nine ribs.

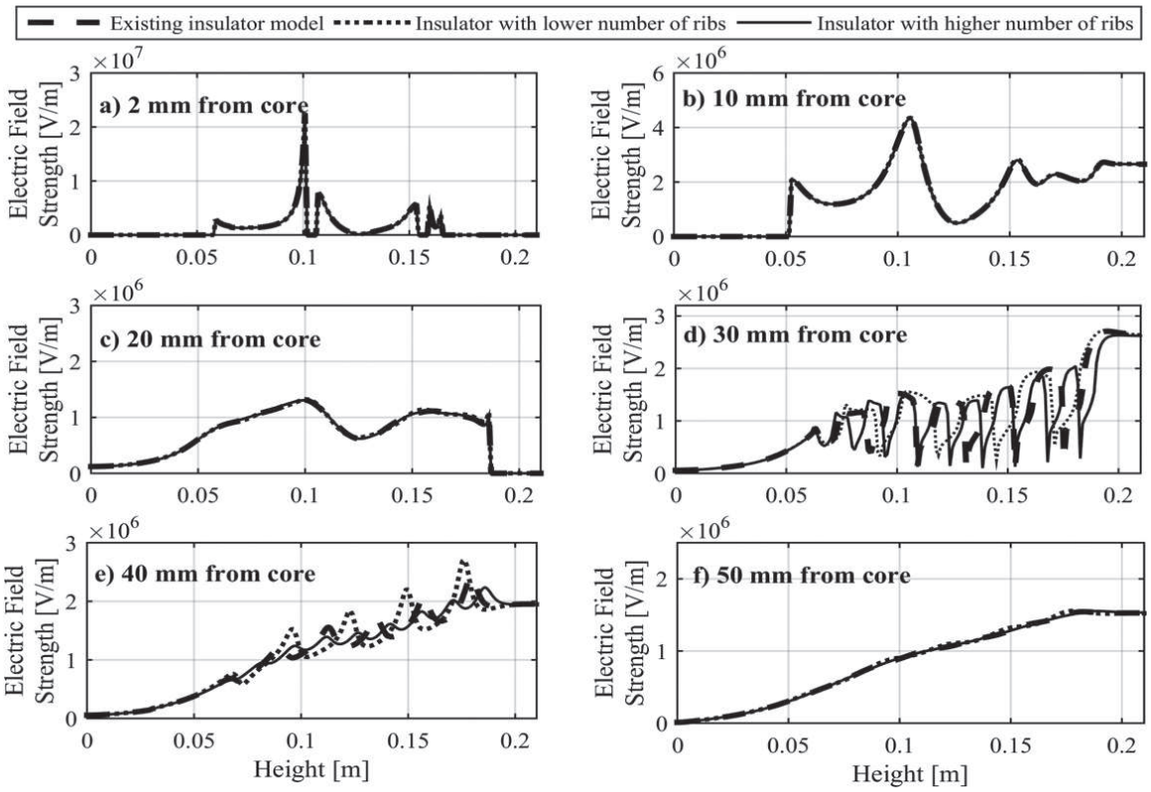

Figure 5. EFS of the MVIPI with five ribs (dotted line), nine ribs (solid line) and the existing MVIPI (dashed line) at different distances from the core of the MVIPI: (a) 2 mm for core, (b) 10 mm from core, (c) 20 mm from core, (d) 30 mm from core, (e) 40 mm from core and (f) 50 mm from core.

4. MVIPI with the exceptional external shape

The following presents the developing MVIPI's new external shape (**Figure 7**). The designed insulator exterior, as such, does not have the characteristically shaped ribs, since it has been acquired by using the Lagrange interpolating polynomial of sixth degree (**Figure 6a**) [2]. Lagrange's interpolating polynomial for a set of $n + 1$ given data points is written in the form (1) [2]:

$$M_n(r) = \sum_{i=0}^{n} G_i(r)\, z_i, \tag{1}$$

while $G_i(r)$ are Lagrange coefficients which is given by (2) [2].

$$G_i(r) = \frac{(r-r_0)(r-r_1)(r-r_2)\cdots(r-r_{i-1})}{(r_i-r_0)(r_i-r_1)(r_i-r_2)\cdots(r_i-r_{i-1})} \cdot \frac{(r-r_{i+1})\cdots(r-r_n)}{(r_i-r_{i+1})\cdots(r_i-r_n)}. \tag{2}$$

Taking into account the short form for the product of the differences (2) in (1) over (3), the final form is acquired for the Lagrange interpolation polynomial (4) [2]

$$\prod_{j=0}^{n}(r-r_j) = (r-r_0)(r-r_1)(r-r_2)\cdot\ldots\cdot(r-r_{j-1})(r-r_j)(r-r_{j+1})\cdots(r-r_n) \tag{3}$$

$$M_n(r) = \prod_{l=0}^{n}(r-r_l)\cdot\sum_{i=0}^{n}\frac{1}{(r-r_i)}\frac{f(r_i)}{\prod_{j=0,j\neq i}^{n}(r_i-r_j)}. \tag{4}$$

For the sixth-degree polynomial, seven points are needed [2], which are labeled with $P_i(r_i, z_i)$, where $i = 0,1,\ldots,6$. Fixed points are $P_0(r_0, z_0)$ and $P_6(r_6, z_6)$: $r_0 := 0.185$ m, $z_0 := 0.029$ m and $r_6 := 0.064$ m, $z_6 := 0.029$ m. Coordinates P_0 and P_6 are marked in **Figure 6a** and **6b**.

The next step is to identify five middle points [2]. Such r_i are selected, subject to $r_0 < r_i < r_6$, where $i = 1,2,\ldots,5$. According to step s (5) [2], values r_1, r_2, r_3, r_4, and r_5 are selected:

$$s = \frac{(r_0 - r_6)}{6} = \frac{(0.185 - 0.064)}{6} = 0.0202 \text{ m}, \tag{5}$$

followed by the calculation of r_1, r_2, r_3, r_4, and r_5:

$$r_i = r_0 - s \cdot j; i = 1, \ldots, 5; j = 1, \ldots, 5. \tag{6}$$

After calculation (6), the next values are obtained: $r_1 = 0.165$ m, $r_2 = 0.145$ m, $r_3 = 0.125$ m, $r_4 = 0.105$ m, and $r_5 = 0.084$ m. Values z_1, z_2, z_3, z_4, and z_5 are determined by considering the creeping distance of the MVIPI, which must not be lower than the original MVIPI. The following state (7) [2] is defined for values z_1, z_2, z_3, z_4, and z_5:

$$z_1, z_2, \ldots, z_5 \geq \begin{cases} z_0 \\ z_6 \end{cases}; \tag{7}$$

therefore, the obtained values are $z_1 = 0.056$ m, $z_2 = 0.033$ m, $z_3 = 0.037$ m, $z_4 = 0.034$ m, and $z_5 = 0.036$ m.

Intermediate polynomials are used before the final polynomial form [2]. For $i = 0,1,2,\ldots,6$ is defined:

$$M_i(r) = \prod_{j=0, j\neq i}^{6} \frac{r - r_j}{r_i - r_j} \tag{8}$$

The sixth-degree polynomial [2] that will go through the points P_0 and P_6 (9) is given as:

$$m(r) = \sum_{i=0}^{6} M_i \cdot z_i = M_0 \cdot z_0 + M_1 \cdot z_1 + M_2 \cdot z_2 + M_3 \cdot z_3 + M_4 \cdot z_4 + M_5 \cdot z_5 + M_6 \cdot z_6. \tag{9}$$

The sixth-degree polynomial that replaces the shape of the MVIPI's ribs is shown in **Figure 6b**.

The MVIPI's novel external shape is shown in **Figure 7**, with the EFS value. **Figure 8** compares EFS values between the existing MVIPI (dashed line) and the MVIPI with the novel external shape (solid line). The values of EFS are within the defined bounds, with the exception of the boundary insulator to air (30 mm from the insulator core), where the EFS value of the MVIPI with the new external shape exceeded the permissible value slightly 3 MV/m (3.28 MV/m). The lowest possible value of EFS is wanted in that area; hence, the coefficients of the polynomial will be optimized with the goal of reducing the EFS at the boundary insulator to air and finding the best position of the internal components of the MVIPI.

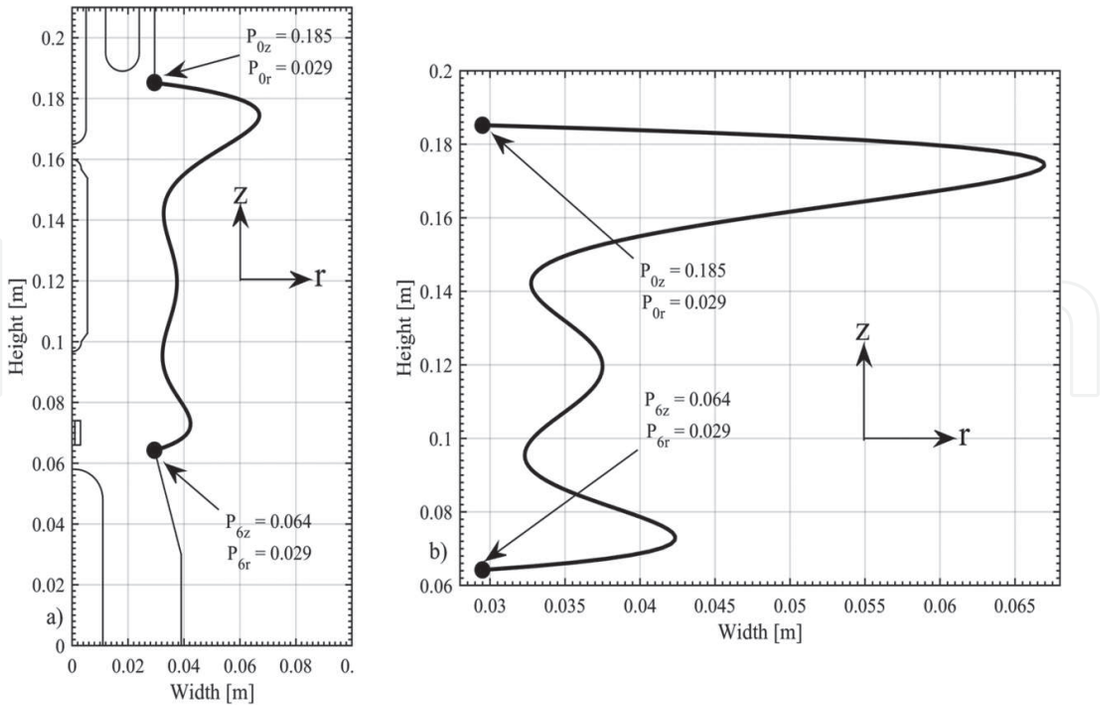

Figure 6. (a) Designed ribs using the sixth-degree polynomial. (b) Sixth-degree polynomial, which describes the exterior of the MVIPI.

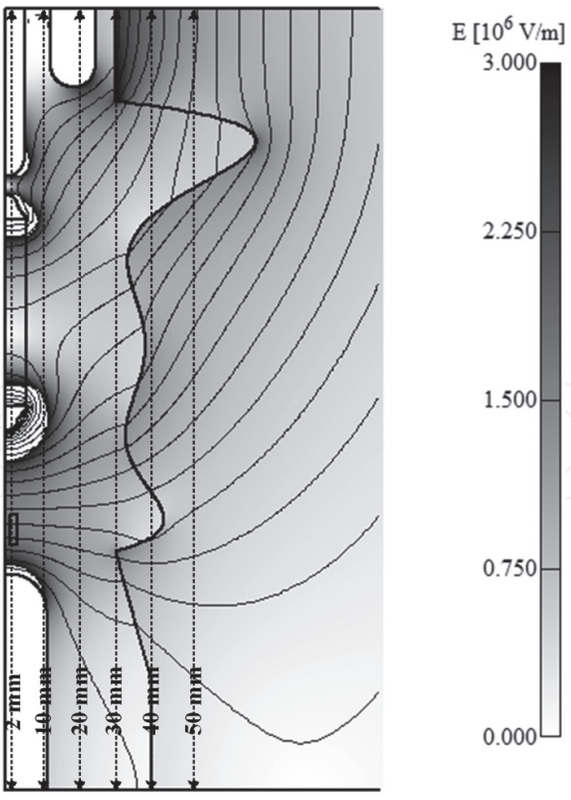

Figure 7. EFS of the MVIPI with the novel external shape.

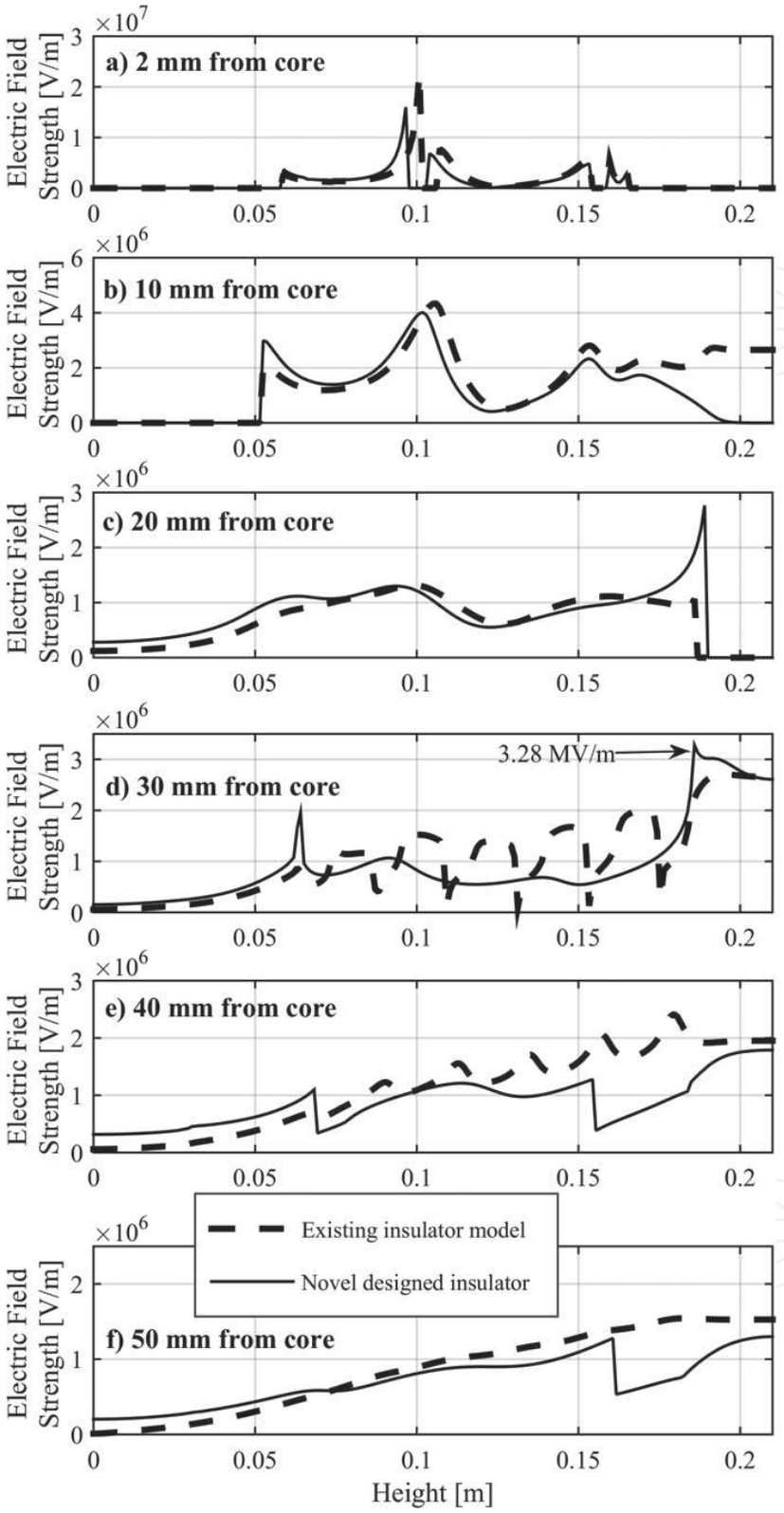

Figure 8. EFS of the MVIPI with the novel external shape (solid line) and the existing MVIPI (dashed line) at different distances from the core of the MVIPI: (a) 2 mm for core, (b) 10 mm from core, (c) 20 mm from core, (d) 30 mm from core, (e) 40 mm from core and (f) 50 mm from core.

5. Best external shape and the position of the internal MVIPI's components' calculation by means of the differential evolution algorithm

DE is a fast and robust population-based direct-search stochastic optimization algorithm that was first introduced by Storn and Price [5]. This algorithm is widespread among engineering audiences [2, 3, 13–17] due to its robustness in reaching global minima, suitable for solving nonlinear and constrained optimization problems. It requires only boundaries of expected solutions and has only a few control parameters to be defined. A detailed description of the DE algorithm is available from [5, 6].

The component to be optimized is written mathematically in the form of an objective function. In this chapter, the criterion of optimizing is the value of EFS in the most stressed points, which are settled in the air just above the insulator-to-air intersection [2], from the top of the insulator through ribs to the bottom of the insulator. The electric field, is in these points, defined as $E = 3$ MV/m, due to the dielectric strength of air, and the goal is to minimize this value to the utmost.

The wanted value E_W of the electric field in the most stressed points has been defined while preparing the objective function, and its value is 2.2 MV/m. This value, 2.2 MV/m, is chosen to obtain a certain reserve with withstand test voltages. Thus, the objective function q [2] is defined with the following statement (10):

$$q = \frac{\max(E_i, \ldots, E_n)}{E_W}; i \in (1, \ldots, n) \tag{10}$$

where $\max(E_i,\ldots,E_n)$ is the maximal value of the EFS in the most stressed points and n is the number of those points.

Due to the optimization process of minimization of the EFS, the parts of the geometric areas of the MVIPI are written parametrically (polynomial coefficients, upper right connector, the distance between the resistor and the bottom electrode). By adjusting the parameters, the shape of the MVIPI will occur in which the value of the electric field is the lowest at critical points. Boundaries are determined by the parameters, within which they will be alternated [2, 3].

In total, there are six parameters that are labeled from p_1 to p_6. Parameters p_1, p_2, and p_3 change the MVIPI's external shape; p_4 changes the distance between the bottom electrode and resistor; and p_5 and p_6 change the height and width of the upper right connector. **Table 2** shows the values of searched parameters before and after optimization, as well as their boundary values (maximum and minimum). **Figure 9** shows searched insulator parameters before and after optimization. The optimization algorithm changed the MVIPI's initial design and searched for the suitable parameters' configuration for the most favorable electric field's distribution. The result of the optimization is a set of best parameters from p_1 to p_6 from **Table 2**. The resulting best values define the MVIPI's external shape and position of internal components, which provide the most favorable electric field's distribution. This result was obtained at the size of the population $NP = 30$ and the following control parameters of the DE algorithm $F = 0.6$; $CR = 0.8$ *strategy* = DE/rand/1/bin.

Parameter	Minimum value	Maximum value	Value before optimization	Value after optimization
p_1	0.041	0.056	0.056	0.044
p_2	0.033	0.043	0.037	0.043
p_3	0.034	0.050	0.036	0.042
p_4	0.070	0.140	0.070	0.070
p_5	0.021	0.038	0.015	0.038
p_6	0.007	0.012	0.012	0.012

Table 2. Parameter values before and after optimization.

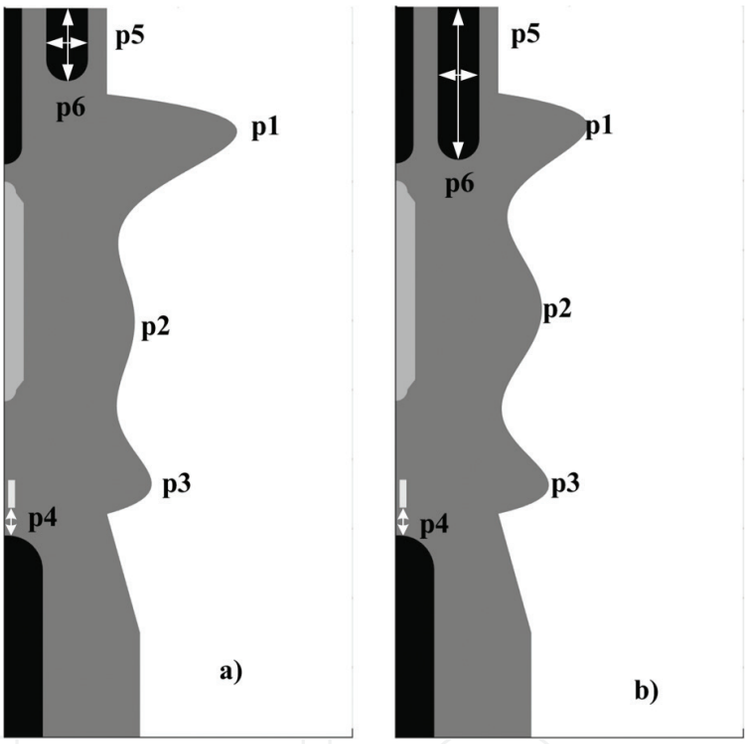

Figure 9. MVIPI parameters: (a) before optimization and (b) after optimization.

Figure 10 shows the MVIPI's EFS distribution after the optimization. **Figure 11** shows EFS at different distances from the center of the MVIPI. The solid line marks the EFS of the novel-designed MVIPI after the optimization. The EFS of the novel-designed MVIPI before the optimization is marked with a dotted line. The EFS of the existing MVIPI is marked with a dashed line.

Comparing the results before the optimization, there was a decrease in the EFS inside the insulator and in the air after the optimization. 30 mm from the MVIPI's core (**Figure 11d**), the EFS does not exceed the value of 2 MV/m on the boundary insulator to air. Comparing EFS value between the novel-designed MVIPI before and after the optimization, there is a 35% decrease in the EFS at the same distance after the optimization. On the other hand, comparing EFS values between the existing MVIPI and novel-designed MVIPI after the optimization, there is a 22% decrease in the EFS at the same distance after the optimization.

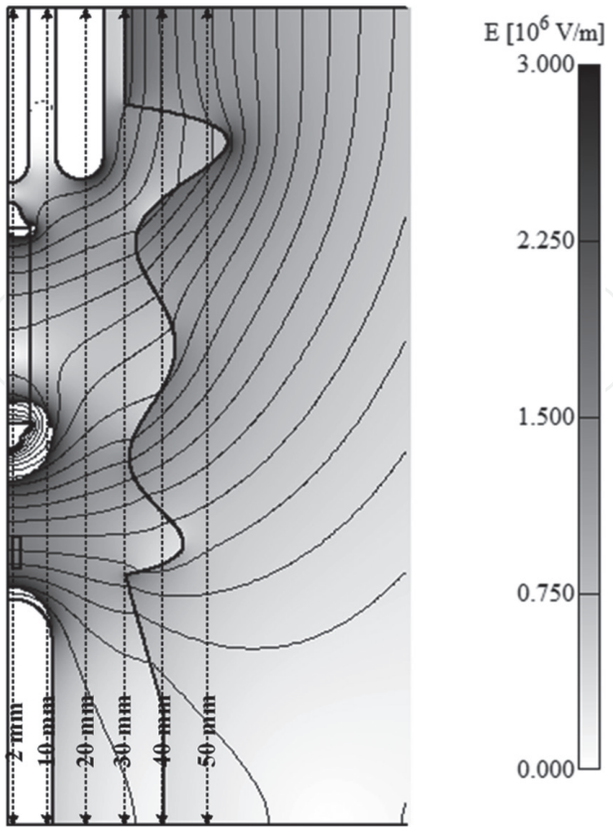

Figure 10. EFS of the MVIPI with the new external shape after the optimization.

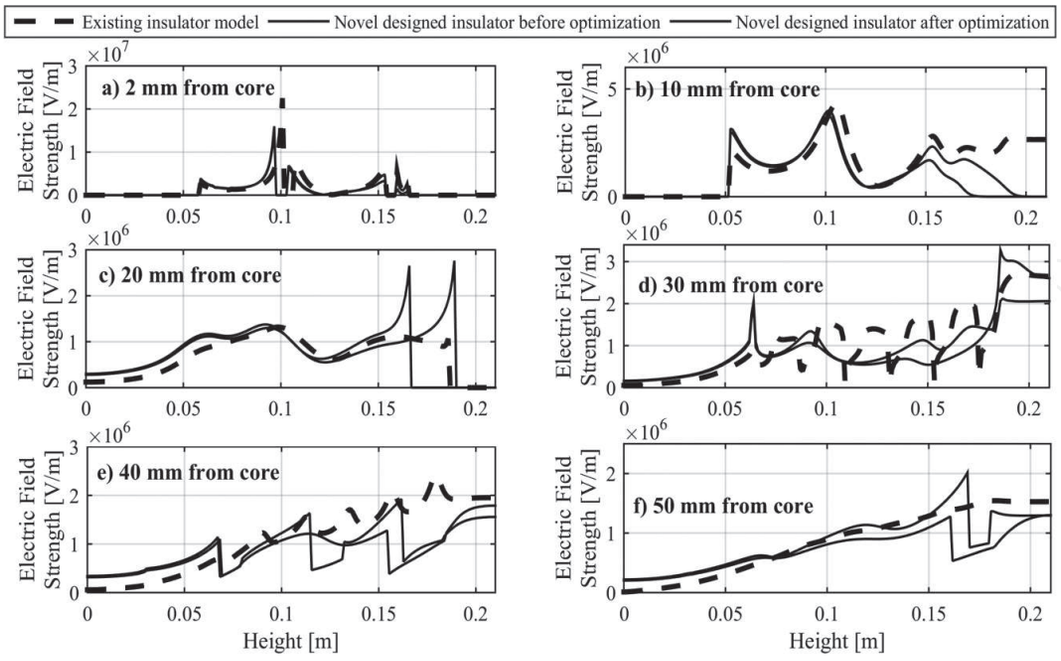

Figure 11. EFS of the novel-designed MVIPI after the optimization (solid line), before the optimization (dotted line) and the existing MVIPI (dashed line) at different distances from the core of the MVIPI: (a) 2 mm for core, (b) 10 mm from core, (c) 20 mm from core, (d) 30 mm from core, (e) 40 mm from core and (f) 50 mm from core.

6. Conclusion

This chapter describes the influence of the electric field on the MVIPI with standard and modified external shapes. The electric field behavior of the MVIPI with different external shapes was shown, and the numerical model was introduced with a favorable distribution of the electric field. The MVIPI's external shape influence on the electric field is researched by means of changing the number of ribs and making a completely new external shape of the MVIPI, which does not have the typical shape of the ribs, but a new outline, using the Lagrange polynomial that has acquired its best form through the optimization process.

The application of the DE algorithm is shown in order to design the MVIPI's external shape and reach the best position of internal insulator elements. It was essential to satisfy the criteria for reaching a certain boundary of EFS inside and in the surrounding area of the MVIPI.

The improved novel-designed insulator, with its modified external shape, is returned mainly in the lower value of the electric field inside the insulator and in the air, which means less exertion of insulation material. Such an MVIPI can function over a long period of time. Producing such an MVIPI is also less challenging, due to the fewer elements inside the insulator and, thus, fewer risks for partial discharges. Another major achievement is scrap decrease, which is economically noteworthy. The tool for molding the MVIPI's external shape is less complex, which is favorable for production and that it will be less possible to form cavities in the casting.

Nomenclature

CR	crossover rate
DE	differential evolution
E	electric field strength [V/m]
E_W	wanted value of the electric field strength [V/m]
F	mutation factor
$G_i(r)$	Lagrange coefficients
i, j	indices
$M_n(r)$; $m(r)$	Lagrange interpolating polynomial
n	number of data points
NP	size of the population
$p_1, \ldots, p_6$	parameters of the insulator

q	objective function
(r, z)	coordinates [m]
s	step [m]
ε_r	dielectric permittivity

Author details

Mirza Sarajlić[1]*, Jože Pihler[1], Nermin Sarajlić[2] and Peter Kitak[1]

*Address all correspondence to: mirza.sarajlic@um.si

1 University of Maribor, Faculty of Electrical Engineering and Computer Science, Maribor, Slovenia

2 University of Tuzla, Faculty of Electrical Engineering, Tuzla, Bosnia and Herzegovina

References

[1] Pihler J. Switchgear of Electric Power System. 2nd ed. Maribor: University of Maribor, Faculty of Electrical Engineering and Computer Science; 2003. pp. 1-273

[2] Sarajlic M, Kitak P, Pihler J. New design of a medium voltage indoor post insulator. IEEE Transactions on Dielectrics and Electrical Insulation. 2017;**24**(2):1162-1168. DOI: 10.1109/TDEI.2017.005947

[3] Sarajlić M, Pihler J. The influence of the number of ribs of a medium voltage post insulator on the electric field. In: 2016 International Symposium on Fundamentals of Electrical Engineering (ISFEE); Bucharest; June 30–July 2 2016. p. 1-5

[4] Tičar I, Kitak P, Pihler J. Design of new medium voltage indicator by means of electric field calculation. Journal of Microelectronics, Electronic Components and Materials. 2002;**32**(2):82-87

[5] Storn R, Price K. Differential evolution—A simple and efficient heuristic for global optimization over continuous spaces. Journal of Global Optimization. 1997;**11**(4):341-359. DOI: 10.1023/A:1008202821328

[6] Price KV, Storn RM, Lampinen J. A. Differential Evolution: A Practical Approach to Global Optimization. 1st ed. Berlin Heidelberg: Springer-Verlag; 2005. p. 539

[7] Program tools EleFAnT. Graz, Austria: Inst. Fundam. TU Graz Theory Electrc. Eng; 2000

[8] Sheikholeslami M, Hayat T, Alsaedi A, Abelman S. Numerical analysis of EHD nanofluid force convective heat transfer considering electric field dependent viscosity. International Journal of Heat and Mass Transfer. 2017 May;**108**:2558-2565

[9] Sheikholeslami M, Soleimani S, Ganji DD. Effect of electric field on hydrothermal behavior of nanofluid in a complex geometry. Journal of Molecular Liquids. 2016 Jan;**213**:153-161

[10] Sheikholeslami M, Ganji DD. Impact of electric field on nanofluid forced convection heat transfer with considering variable properties. Journal of Molecular Liquids. 2017 Mar;**229**:566-573

[11] IEC 61958:2000. High-voltage Prefabricated Switchgear and Controlgear Assemblies—Voltage Presence Indicating Systems. 1st ed.; 2000

[12] IEC 61243-5:1997. Live Working—Voltage Detectors—Part 5: Voltage Detecting Systems (VDS). 1st ed.; 1997

[13] Sarajlić M, Pocajt M, Kitak P, Pihler J. Bare conductor temperature coefficient calculation by means of improved differential evolution algorithms. In: Maribor: 13th Slovenian Power Engineering Conference CIGRE-CIRED; 22-24 May 2017. p. 1-10

[14] Sarajlić M, Pocajt M, Kitak P, Sarajlić N, Pihler J. Covered overhead conductor temperature coefficient calculation using differential evolution optimization algorithm. In: Neum: 13th BH K CIGRE Power Engineering Conference; 17-21 September 2017. p. 1-11

[15] Glotic A, Pihler J, Ribic J, Stumberger G. Determining a gas-discharge arrester model's parameters by measurements and optimization. IEEE Transactions on Power Delivery. 2010;**25**(2):747-754

[16] Glotić A, Glotić A, Kitak P, Pihler J, Tičar I. Optimization of hydro energy storage plants by using differential evolution algorithm. Energy. 2014 Dec;**77**:97-107

[17] Glotic A, Sarajlic N, Kasumovic M, Tesanovic M, Sarajlic M, Pihler J. Identification of thermal parameters for transformer FEM model by differential evolution optimization algorithm. In: 2016 International Conference Multidisciplinary Engineering Design Optimization (MEDO). 2016. pp. 1-6

IntechOpen

IntechOpen

IntechOpen